Materials & Design 232 (2023) 112115

Contents lists available at ScienceDirect

Materials & Design

journal homepage: www.elsevier.com/locate/matdes

Polydimethylsiloxane based soft polymer optical fibers: From the processing-property relationship to pressure sensing applications

Khushdeep Sharma [a,c], Elodie Morlec [a], Sebastian Valet [b], Martin Camenzind [a], Bernhard Weisse [b], René M. Rossi [a], Fabien Sorin [c], Luciano F. Boesel [a,*]

[a] Empa, Swiss Federal Laboratories for Material Science and Technology, Laboratory for Biomimetic Membranes and Textiles, Lerchenfeldstrasse 5, 9014 St.Gallen, Switzerland
[b] Empa, Swiss Federal Laboratories for Material Science and Technology, Laboratory for Mechanical Systems Engineering, Ueberlandstrasse 129, 8600 Duebendorf, Switzerland
[c] EPFL, Laboratory of Photonic Materials and Fibre Devices, MXG 335 (Bâtiment MXG), Station 12, CH-1015 Lausanne, Switzerland

HIGHLIGHTS

- Moulding and dip coating processes were developed for the production of Polydimethylsiloxane (PDMS) based polymer optical fibres (POFs).
- Mechanical and optical properties of PDMS POFs can be tuned on-demand by judicious selection of composition and process parameters.
- PDMS POFs can sense loads as low as 0.1 N.
- PDMS POFs provide continuous sensing of pressures under constant and cyclic conditions.

GRAPHICAL ABSTRACT

Photonic textile sensors were designed with tailor-made, soft polymer optical fibers able to sense pressure in the range of 40kPa – 350kPa

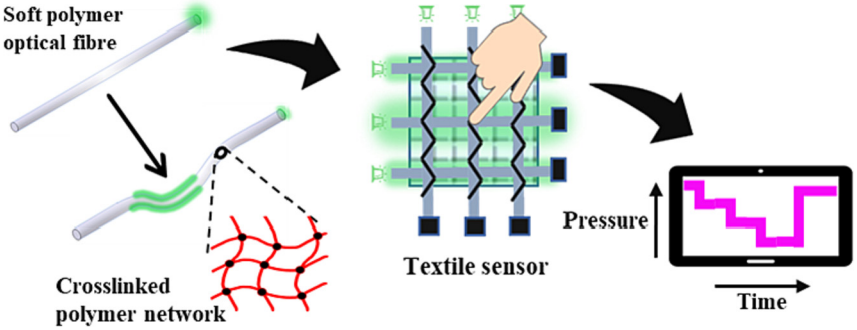

ARTICLE INFO

Article history:
Received 13 December 2022
Revised 19 June 2023
Accepted 22 June 2023
Available online 25 June 2023

Keywords:
Base to crosslinker ratio
Tensile modulus
Light attenuation
Pressure sensing

ABSTRACT

Polydimethylsiloxane (PDMS) based soft polymer optical fibers (POFs) have recently demonstrated their intriguing potential for different sensing applications like strain or temperature sensing. Recent studies have elaborated on the sensing capability of PDMS POFs, yet the in-depth analysis of the processing-property relationship of PDMS POFs remains unexplored. A straightforward processing strategy was developed for core only PDMS POFs and PDMS/THV (terpolymer of tetrafluoroethylene, hexafluoropropylene, and vinylidene fluoride) core/clad POFs. The optimization of chemical formulations and process parameters such as curing temperature and curing time provided the development of POFs with tailored mechanical and optical properties. The tensile modulus of the moulded PDMS POFs could be tuned in the range of 0.2–3.0 MPa, with attenuations as low as 0.11 dB/cm in the near infrared region (NIR). Furthermore, the load and pressure sensing capability of the PDMS POFs was demonstrated with sensitivity to loads as low as 0.1 N and highly accurate pressure sensing up to 300 kPa. The systematic approach presented in this study enables the processing of elastic PDMS POFs with tunable mechanical and optical properties, which can be tailored to suitable sensing applications in the field of healthcare monitoring, biomedicine, and soft robotics.

* Corresponding author.
E-mail address: luciano.boesel@empa.ch (L.F. Boesel).

https://doi.org/10.1016/j.matdes.2023.112115
0264-1275/

1. Introduction

Polymer optical fibers (POFs) are envisionned as ideal candidates for applications in short-range data transmission, illumination, and sensing. In particular, POF based sensing provides an alternative approach to electronic sensing with the advantages of the absence of electrical noise, and shielding against electromagnetic interference [1–3]. Optical sensors especially in the form of wearable health monitoring devices are expected to improve and provide better healthcare opportunities [4]. Soft and stretchable POF based sensors provide a facile and versatile approach to continuously sense a variety of physiological parameters of the human body, such as heart rate, pressure, oxygen saturation, strain, body movements, and breathing rate of patients in real-time [5–8]. The POFs can be integrated into smart textiles that can act as mobile and wearable healthcare (m-health) units for personalized health monitoring of patients [2]. In our previous works, we have demonstrated various POF based wearable sensors [9–12]. One of our recent studies demonstrated the melt spinning of monofilament urethane-siloaxne co-polymer (Geniomer) based POFs for pressure sensing applications [12]. The textile integrated Geniomer POFs enabled the successful measurement of the desired pressure [12].

The polymers used for the processing of POFs should satisfy specific mechanical and optical requirements in order to be utilized in the aforementioned applications. In particular, they must exhibit high optical transparency within some wavelength range, and have mechanical properties that combines softness with a strength high enough to withstand the forces during the textile integration processes. Among the potential candidates, elastomers such as PDMS-based resins, possess high transparency in the visible and near-infrared region, and can be tailored to exhibit very low tensile modulus [13,14] as compared to their traditional rigid counterparts such as poly(methyl methacrylate) (PMMA) or polycarbonate (PC) [15]. Moreover, low refractive index fluoropolymers such as THV (terpolymer of tetrafluoroethylene, hexafluoropropylene, and vinylidene fluoride) can be utilized as the cladding material [16] in combination with PDMS core.

Thus far, however, the fabrication challenges associated with processing and shaping thermally crosslinkable polymers remain for a large part unresolved. Indeed, PDMS-based soft polymer materials require specific processing approaches to realize optical fibers due to their thermally crosslinkable nature. In particular, the traditional POF processing methods, such as bicomponent melt spinning [17], co-extrusion [18], and thermal drawing [19], cannot be utilized. Moulding is one of the prominent strategies for processing POFs from thermally crosslinkable polymer system and could also be applied for the development of PDMS POFs [20]. However to date, few studies exist on the the moulding of thermally crosslinkable PDMS POFs [15,20–22], and none have investigated in depth the processing-property relationship to achieve lower losses and better output. Flipsen et.al. demonstrated the earliest study on the processing of polycarbosiloxanes based POFs [21]. They utilized moulding of a polycarbosiloxanes formulation in FEP (Fluorinated ethylene propylene) tubing, and in this study, POFs were not demoulded but rather the FEP tubing was used as a cladding [21]. Guo et al. developed stretchable PDMS based polymer optical fibers for strain sensing applications [15]. They reported flexible PDMS based optical fibers doped with dye (Rhodamine B) for the design of human motion sensors. The fiber enabled sensing of different motions of the human body, which were quantified as a function of the absorbance of light by the dye versus the strain subjected to the fiber. The undoped PDMS fibers showed light attenuation of 0.51 dB/cm and doped fibers depicted light loss of 3.02 dB/cm [15]. In another recent study, Guo et al. reported the development of temperature-sensitive elastomeric POFs, which were also processed by moulding. The temperature sensing function was incorporated by doping upconverting nanoparticles (UCNPs) in the elastomer formulation [22]. Despite these interesting developments, a comprehensive study including processing-property relationship of PDMS POFs is still missing, that would provide important new knowledge and opportunities for the further development of this novel class of elastomeric optical fibers [23]. Among the reported studies on PDMS POFs, none of them described the effect of base to crosslinker ratio and curing temperature on the processability and light attenuation. Especially, PDMS POFs with base to crosslinker ratio (1:1), (15:1) and (20:1) have not been reported in any study. The optimization of the mechanical and optical properties of PDMS POFs will allow in particular for better sensing performance and the feasibility of faster fabrication, and upscaling for a variety of sensory applications.

In this study, the processing-property relationship of soft POFs via different characterization approaches has been revealed. The effect of the chemical formulation of PDMS, curing temperature, and crosslink density on the mechanical and optical properties of POFs have been studied in detail. The processing parameters established in our study have allowed us to tailor the tensile modulus of the POFs on demand. For example, PDMS POFs with formulation (1:1) and (20:1) provide the POFs with tensile modulus as low as $\approx$ 0.5 MPa, which is in the stiffness range of human skin. Moreover, as also shown in this study, curing temperature applied for the processing of PDMS POFs also holds an advantage for certain sensory applications. For example, the formulation PDMS POFs (10:1) cured at room temperatures, can be incorporated with various different additives such as thermally sensitive biomolecules to develop novel biosensors. The room temperature curing also eliminates the use of an oven, making the moulding process environmentally friendly from an energy point of view.

This study achieved among the lowest reported optical light attenuation of PDMS POFs with excellent mechanical deformability, using a controlled process. Besides core only PDMS POFs, this work also demonstrated the development of new material combination PDMS/THV (core/clad) POFs via the dip coating process for the first time.

Furthermore, the ability to precisely control the mechanical properties of the soft POFs can be utilized to create exciting opportunities for the integration of soft PDMS POFs into the textiles. The successful integration of PDMS POFs into a textile patch and the further development of wearable pressure sensor was also shown in this work. Finally, the effect of environmental factors on the optical performance of the soft PDMS POFs and the real-time sensing performance of the textile integrated PDMS POFs was demonstrated in this work. The soft POFs and processing platforms developed in this work will pave the way toward novel opportunities for sensing via smart textiles and soft robotics.

2. Experimental section

2.1. Materials and methods

The PDMS based silicone elastomer (SYLGARD™ 184, Dow®) was used as the core material for processing of the POFs. The fluoro-thermoplastic THV 221AZ (3M™, Dyneon™) was used as the cladding material for the processing of the PDMS/THV (core/-clad) POFs. The 10 (w/v %) polymer solution of THV (terpolymer of tetrafluoroethylene, hexafluoropropylene, and vinylidene fluoride) was prepared by dissolving it in acetone. This polymer solution of THV in acetone was utilized for the dip coating of PDMS core only POFs.

The formulations with different base to crosslinker ratios were prepared as mentioned in Table 1. A fluoroplastic tube (PTFE) of internal diameter 1000 μm was used as the mould material. Moulding was used as the method for the processing of PDMS based polymer optical fibers (POFs).

The process started with the preparation of the PDMS formulation in a specific ratio of base to crosslinker. For example, 10:1 formulation implies 10 parts of base by weight and 1 part of crosslinker by weight. The five different formulations, namely, 1:1, 5:1, 10:1, 15:1, 20:1, were prepared. The base and crosslinker were weighed in a plastic beaker. The polysiloxane formulation was mixed thoroughly, followed by centrifugation to ensure the bubble free transparent formulation. Then, each formulation was carefully loaded into the prepared syringe-needle system. The formulations were filled in the tubular PTFE mould via attachment of the syringe-needle system and were cured at a curing temperature of 125 °C for 37 min (see Fig. S15 for a discussion on the rationale for choosing these values, whereas S15 implies Fig. S15 in Supporting Information). After the curing step, the POFs were allowed to cool at room temperature and were demoulded from the tubular PTFE mould. Fig. 1a describes the schematic of the moulding method for the processing of the core only POFs.

The PDMS core only POFs were also processed via moulding by the variation of the curing temperature at a fixed base to crosslinker ratio of 10:1. The PDMS POFs were cured at the curing temperatures of 23 °C, 75 °C, 125 °C, and 200 °C for 96 h, 2.5 h, 37 min, and 22 min, respectively (see Fig. S16 for details on chosing curing parameters via rheological investigation of PDMS formulations).

The PDMS POFs (10:1) cured at 125 °C for 37 min were selected for the dip coating process, owing to their good mechanical and optical properties compared to the other PDMS POFs developed in this study. The PDMS POF specimens with a length in the range of 55–60 cm were cut for the dip coating process. The samples were cleaned with ethanol to get rid of dust particles from the surface of the PDMS POFs. The automated robotic arm dip coater device (RDC 15 with Stepper Motor Control, Bungard Elektronik Gmbh & Co. KG, Germany) was used for the vertical dip coating of the POFs in the THV polymer solution. The POFs were dip coated with a withdrawal speed of 11.3 mm/s for a dip time of 60 s in the THV solution. These parameters were selected according to the results from Table S3 (S3 implies Table S3 in Supporting information), as they provided the desired THV cladding thickness. After the dip coating process, solvent evaporation led to formation of a thin transparent THV cladding around the PDMS core. The dip coated PDMS/THV (core/clad) POFs were annealed in the oven at 110 °C for 20 min to ensure the complete removal of the solvent acetone from the THV cladding. Fig. 1b describes the schematic of the dip coating process for the development of the core/clad (PDMS/THV) POFs.

Table 1
Processing parameters utilized for the moulding of PDMS core only POFs by changing the base to crosslinker ratio of the PDMS elastomer.

Sample Name	Base to Crosslinker ratio (by weight)	Cure Temperature (°C)	Curing Time (min)
PDMS POF (1:1)	1:1	125	37
PDMS POF (5:1)	5:1	125	37
PDMS POF (10:1)	10:1	125	37
PDMS POF (15:1)	15:1	125	37
PDMS POF (20:1)	20:1	125	37

2.2. Characterization of PDMS POFs

An optical microscope (Keyence 1000 series) was used to study the diameter of the PDMS based POFs. The cross-section of the moulded PDMS fiber was prepared with the help of a normal optical fiber cutter blade. The mechanical properties of the PDMS POFs were characterized using single fiber tensile tester (Textechno Statimat ME). The gauge length of each fiber specimen was 50 mm and the test speed used was 100 mm/min. At least seven specimens were tested for each sample.

Light light attenuation of the PDMS POFs was studied using the standard cut back technique at the wavelength of 455 nm, 530 nm, 660 nm, and 810 nm. The length of each specimen for the test was in the range of 60–70 cm and at least three specimens were tested for each type of POF. The fiber coupled LEDs (Thorlabs, Inc.) M455F3, M530F2, M660FP1, and M810 F2 were used as light sources in the cut back setup. For the calculation of the coefficient of light attenuation (α), 5 cuts were made along the length of each PDMS POF specimen at a distance of 5 cm, 10 cm, 20 cm, 30 cm, and 40 cm. The coefficient of light attenuation was calculated using Eq. (1).

$$\propto = \frac{10}{L_2 - L_1} \log\left(\frac{P_1}{P_2}\right) \quad (1)$$

where α is the light attenuation in dB/cm, L_1 and L_2 are initial and final length of the fiber in cm, respectively, and P_1 and P_2 are the initial power output before the cut and the final power output in pA after the cut, respectively.

Infrared (IR) spectroscopy of the PDMS POFs was performed using a Bruker Tensor 27 system integrated with a GladiATR™ single reflection ATR accessory. A diamond crystal was used for the measurements of the PDMS POF samples. The PDMS POFs were pressed against the crystal, and absorbance spectra were recorded in the spectral range of 4000–450 cm^{-1} with a sample scan of 64 and a resolution of 4 cm^{-1}. OPUS 8.1 software package was used for the analysis of the IR spectra, and all the spectra were baseline corrected for qualitative comparative analysis of the crosslinker in the PDMS POFs.

Atomic force microscopy (AFM, Nanosurf C-3000, Nanosurf AG) was performed in dynamic mode to characterize the surface roughness of the Teflon mould and PDMS POFs. The AFM tip Tap 150 AI-G (Budget Sensors) with a spring constant of 5 N/m was used for scanning the samples. The scan was done for the area of 10 μm × 10 μm for both types of samples.

The swelling study of core only PDMS POFs was done utilizing the solvent toluene at room temperature (23 °C). The solvent toluene used in the experiment was purchased from Biosolve (CAS: 108–88-3). The density of toluene as provided by the supplier was 0.87 g/cm^3 and the density of PDMS POFs was in the range of 1.04–1.08 g/cm^3 (SI, Table S4). First, pre-swelling of the POFs was done to extract the uncrosslinked portion of the polymer chains (sol fraction) present in the polymer network into the solvent. The initial mass of the POFs was measured before the pre-swelling. Then, the POFs were immersed in toluene for 25 h for the pre-swelling experiment. The final mass of the POFs was measured after drying the POFs under the hood for 4 days at room temperature. The sol fraction present in the crosslinked PDMS POFs was calculated using equation (2).

$$\%\, Sol\, Fraction = \frac{m - m_{dry}}{m} * 100 \quad (2)$$

where m is the mass of the PDMS POF before swelling and m_{dry} is the mass of the PDMS POF after drying.

The dried PDMS POF specimens from the pre-swelling study were subjected to a final swelling test. The POFs were immersed in toluene for 90 h. For the measurement of the final mass of the

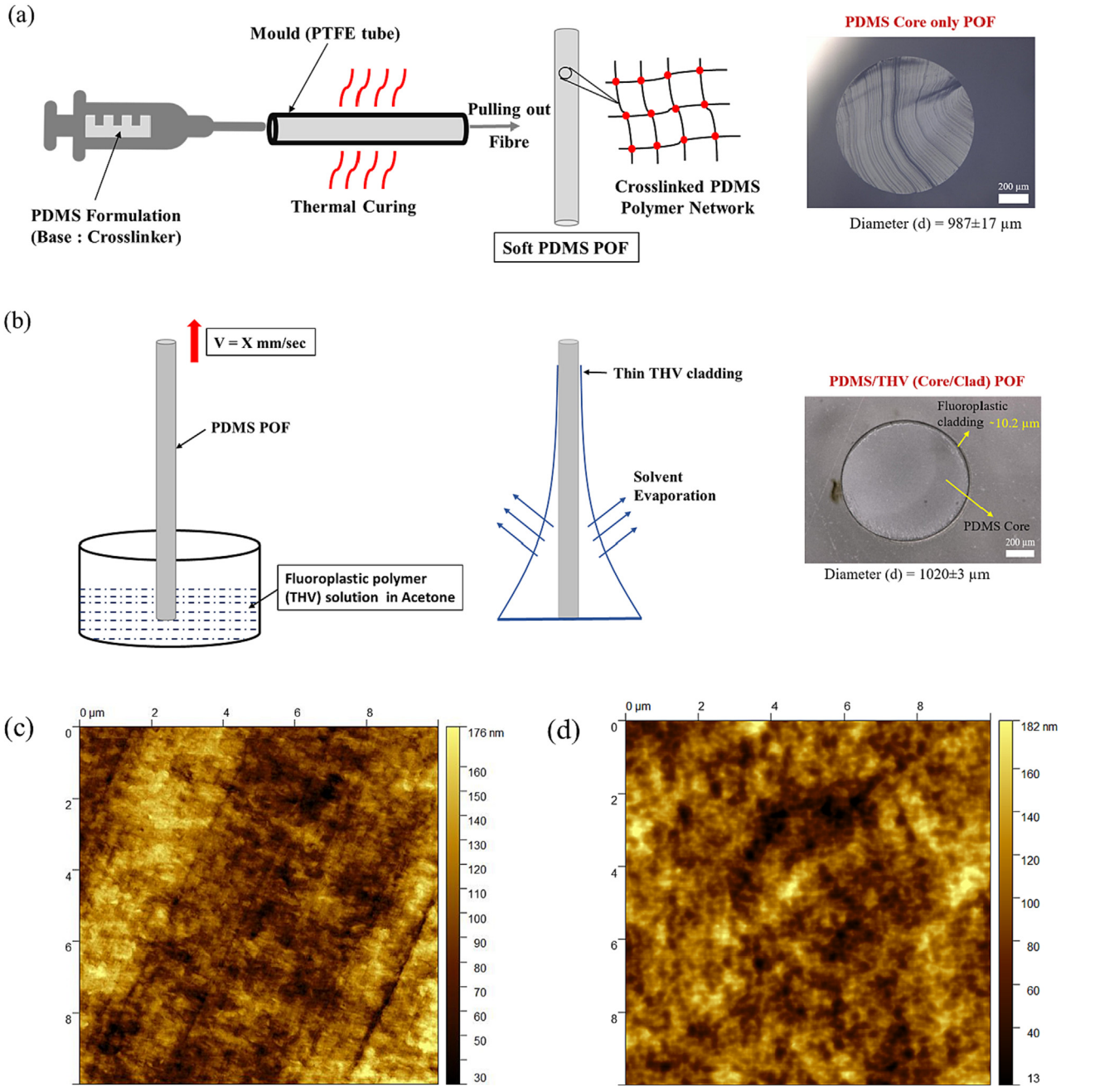

Fig. 1. Processing of elastomeric POFs. a) Moulding strategy for the processing of the core only PDMS POFs in PTFE tube based moulds. b) Dip coating of PDMS based core only POFs in a THV polymer solution to process PDMS/THV (core/clad) POFs. The dip coating process led to the formation of a thin cladding (~10 µm) around the PDMS core. c) Topography acquired in AFM tapping mode for the inside wall of the PTFE tube mould used for processing of POFs. d) Topography acquired in tapping mode for the outer surface of the processed PDMS POF (10:1).

swollen POFs (m_{sw}), the surface of the POFs was wiped quickly with tissue to remove excess solvent from the surface and then the fibers were immediately weighed. The crosslink density of the PDMS POFs was calculated using the Flory-Rehner approach. The equilibrium degree of swelling of PDMS was calculated by applying Eq. (3), whereas the volume fraction dependent Flory-Huggins interaction parameter was calculated by applying Eq. (4) [24]. Furthermore, the crosslink density of the PDMS POFs was calculated by using Eq. (5) [24].

$$Q = \frac{1}{\phi_p} = \frac{V_{sw}}{Vdry} = \frac{\frac{m_{dry}}{\rho_p} + \frac{(m_{sw} - m_{dry})}{\rho_s}}{\frac{m_{dry}}{\rho_p}} \tag{3}$$

$$\chi = 0.459 + 0.134\phi_p + 0.59\,{\phi_p}^2 \tag{4}$$

$$\upsilon = \frac{-log_e(1-\phi_p) + \phi_p + \chi{\phi_p}^2}{V_s\left({\phi_p}^{1/3} - \left(\frac{\phi_p}{2}\right)\right)} \tag{5}$$

where,

Q = Equilibrium Degree of Swelling

ϕ_p = Volume fraction of polymer in swollen network

ρ_p = Density of the Polymer $(g\,.\,cm^{-3})$

ρ_s = Density of the Solvent $(g\,.\,cm^{-3})$

V_s = Molar volume of the solvent $(cm^3.mol^{-1})$

υ = Crosslink Density $(mol\,.cm^{-3}$

Vsw = Volume of swollen POF

Vdry = Volume of unswollen POF

χ = Flory − Huggins (polymer/liquid) interaction parameter

2.3. Textile integration and sensor characterization

2.3.1. Textile integration of POFs

A pressure patch sample was made with PDMS POFs and jacketed commercial PMMA POFs (SH 4001, polyethylene jacketed Super Eska™, inner core diameter (ID) of 1.0 mm, outer diameter (OD) of 2.2 mm ± 0.07 mm (Industrial Fiber Optics, Tampa, AZ, USA). Six pieces of POFs with a 7 cm length were cut and glued to both ends with 1 m of PMMA fibers. The prepared PDMS and PMMA jacketed POFs were placed on top of the textile in order to form a matrix of 3 × 3 fibers. The prepared POFs were integrated to a textile patch via embroidery with a height of the stitches set to 4 mm. The computerized embroidery machine was employed for this process, which was equipped with a framing system that holds the framed area of fabric taut under the sewing needle. The embroidery machine moves the frame automatically and creates a design from a pre-downloaded digital embroidery pattern. The prepared POFs were placed on the base material (textile) and fixed with tape. Fig. S1 shows the digital embroidery pattern that was used to maintain the POFs in order to make the pressure patch. This embroidery process provided the advantage of keeping the POFs in a straight orientation, i.e., less bending losses during the optical measurements. An identical pressure patch sample was also made with the PDMS/THV (core/clad) POFs.

2.3.2. Temperature and humidity sensitivity

The temperature (T) and relative humidity (RH) tests were conducted in a climatic chamber. 20 cm pieces of the following fibers were cut with a normal optical fiber cutter: PDMS core-only and PDMS/THV POFs with a diameter of approximately 1000 μm and 1020 μm, respectively, and jacketed PMMA with an inner core diameter (ID) of 1.0 mm and an outer diameter (OD) of 2.2 mm. The custom built optical transducer device (Fig. S2) equipped with six infrared IF E91D LED (peak wavelength = 870 nm) and six IF D92 phototransistors (peak sensitivity = 870 nm) was used for the optical measurements. Each channel of this device consists of a transmitter and a corresponding receiver, which are connected by a fiber-optic sensor. The user interacts with the measurement device via a graphical user interface built on MATLAB software. The parameters and the recording command are transmitted via USB to the measurement electronics. The reduced light intensity is recorded at the receiver and acquired data represent voltage values in the range of 0 to 2 V. The device's LEDs were switched on for at least 1 h before the first measurements were made, thus avoiding any drift in the device due to the warming up of the electronics. Three measurement repetitions were done by changing the fibers for each repetition. The experiments were performed in steps of increasing or decreasing T/RH, as described in Tables 2 and 3 below.

2.3.2.1. Water droplet test. The water droplet test was operated inside a climatic chamber, in which the temperature and humidity were kept constant at 25 °C and 65%, respectively. The PDMS Core-only POFs and PDMS/THV POFs were connected to the optical transducer device. This optical device is protected with a plastic case on the top of it to avoid water on the components. A sprayer was filled with deionized water conditioned to a temperature of 25 °C. The fibers were placed on a glass plate and 10 mL of water was sprayed on the top surface of the POFs from a distance of approximately 20 cm. Three replicates were performed for each sample.

2.3.2.2. Short and long term measurement. The short and long-term load/pressure measurements were conducted with the "Dickenmessgerät FRANK 16502". This device allows the application of a static pressure with stamps of predetermined mass. For our experiments, a stamp with a diameter of 16 mm was chosen, which allowed the whole surface of the fibers to be touched. The samples were placed under the stamp in order to apply the load in the middle of the POFs. The short-term measurements were performed according to Table 4. The long-term measurements ran for 15 h under a load of 372 g.

2.3.3. Real time PDMS POF sensor test

The pressure patch was placed on the chair covered with the textile (Fig. S3). The duration of the measurement was set to 120 min. The measurement was started without a load, and after 5 min, the human being as the subject applied a pressure/load on the PDMS POFs by sitting on the chair in a normal sitting posture. Before the last 5 min of the measurement, the subject stood up from the chair, i.e., from the demonstrator patch.

2.3.4. Opto-mechanical test protocol: compressive cycling loading

The force and pressure sensing capability of PDMS POFs were tested with the cyclic compression test. The cyclic compression test setup was custom-built by providing the mechanical loading onto the polymer optical fibre during the light transmission process. The PDMS and PDMS/THV POFs of length 55 mm were used as sensing element in this test. Both ends of PDMS POFs and PDMS/THV POFs were connected to the commercial PMMA POFs with the aid of shrink tubing. The whole fibre system was connected on one side to the light source (Fibre coupled LED, 660 nm, Thorlabs, Inc.) and on the other side to the photodetector. The loading on the specific surface area of soft POFs was performed utilizing a metallic cylindrical plunger with a diameter of 16 mm. The complete opto-mechanical setup utilized to determine the sensing performance of PDMS POFs has been described in Fig. S17.

The cyclic compressive loading was performed in a spindle-driven quasi-static test machine of type Z010 from Zwick Roell (Ulm, Germany), equipped with a 20 N load cell. Stress–strain curves were calculated from the test data and correlated with the optical signal data. In a first quasi-static staircase loading test (C1) fibres were loaded to iteratively increased load levels of 0.1 N, 0.2 N, 0.4 N, 0.6 N, 0.8 N, 1.0 N, 1.5, 2.0, 2.5, 3.0, 3.5, 4.0, 4.5 and 5.0 N, respectively as illustrated in Fig. S18.

Secondly, a test with (C2) was performed at a load level of 0.1 N, 1.0 N and 5.0 N, at each level with 10 cycles as illustrated in Fig. S19. Loading conditions for both tests were identical: preload 0.05 N, loading and unloading with displacement-driven mode at 10 mm/min, holding time of 5 s at each load level, and relaxation time of 30 s after each unloading. The compression strain was calculated by plunger displacement with respect to plate-to-plate distance at preload ($\varepsilon = 100 \times \Delta s/ D_0$, Δs: relative displacement, D_0: initial plate-to-plate distance at preload). The compressive stress was calculated with the plunger load with respect to the approximated effective cross-sectional area (Project Diameter of POF × 16.

Table 2
Temperature variation subjected to PDMS, PDMS/THV, and PMMA jacketed POFs. Humidity was kept constant at 55% during this temperature test.

Time (h)	1	2	3	4	5	6	7	8	9	10	11
T (°C)	30	33	36	39	42	45	42	39	36	33	30

Table 3
Humidity variation subjected to PDMS, PDMS/THV, and PMMA jacketed POFs. Temperature was kept constant at 25 °C during the humidity test.

Time (h)	1	2	3	4	5	6	7
RH (%)	40	55	70	85	70	55	40

Table 4
Short term static load measurements conducted for PDMS POFs.

Time (min)	2	4	6	8	10	12
Load (g)	0	167.1	241.1	297.2	371.8	0

0 mm). The details of stress–strain curves of POFs under compression can be seen in Fig. S20.

Further, to estimate the applied pressure on POFs during compressive loading (Fig. S18), the effective contact surface area between soft PDMS POF and the circular plunger was determined via finite element modelling (FEM). The details of FEM are provided in SI on page 17–19.

2.4. Statistical analysis

All the statistical analysis was performed with the R program (v 4.2.0) and R-commander package (v 2.7–2). We initially checked the assumptions of normality and homogeneity of variances by applying the Shapiro Wilk's and Levene's tests, respectively. Deviations from the assumptions were assumed if the tests resulted very significant ($p < 0.01$). In case the samples followed the normality assumption, a one-way ANOVA test (assuming homogeneous or heterogeneous variances, according to the result of the Levene's test) was used to test for the significance effect of one parameter on the property of interest. Tukey contrasts were then used for the comparison of means in case of significant effects. In case the samples did not follow the normality assumption, the respective non-parametric test was used: one-way Kruskal-Wallis' rank sum test followed by a Dunn's test for the comparison of means. For the analysis of the results shown in Tables S1 and S2, a mixed ANOVA test was used to test for the effect of the fiber type (between-subjects factor) and either temperature or RH (within-subjects factor). If significant effects were found, one-way ANOVA tests were performed on the between-subjects factor for each within-subjects factor, followed by pairwise comparison of means for the between-subjects factor.

3. Results and discussion

3.1. Processing of POFs

The core only soft PDMS POFs were processed via moulding with different formulations namely (1:1), (5:1), (10:1), (15:1), and (20:1) by changing the base to crosslinker ratio (refer to details of process in section 2.1 Materials and Methods).

The surface roughness of the inside walls of the tubular mould is an important processing parameter that can influence the surface roughness and optical properties of the final processed PDMS POFs. Fig. 1c and d describe the tapping mode AFM image of the inside wall of the PTFE mould and the outer surface of the PDMS POF (10:1), respectively.

The surface of the PTFE mould possessed a root mean square roughness (RMS) of 27 ± 3.4 nm, whereas the surface of the PDMS POF possessed a RMS roughness of 27 ± 5.2 nm. The roughness profiles of the PTFE mould and the PDMS POF in Fig. S4 provided evidence that the final surface roughness of PDMS POFs was highly dependent on the surface roughness of the tubular mould material.

3.2. Mechanical properties of POFs

The mechanical properties of PDMS POFs were altered by changing the base to crosslinker ratio (Fig. 2a and Table 5). It was found that the POF formulation (10:1) resulted in the highest mechanical strength. Increasing the base to crosslinker ratio in the case of POF formulations (1:1) and (5:1), as well as decreasing the base to crosslinker ratio in the case of POF formulations (15:1) and (20:1) resulted in the decline of the mechanical strength when compared to the POF formulation (10:1). Especially, it was observed that a higher amount of crosslinker in the PDMS POFs (1:1) led to the deterioration of the mechanical properties. However, decreasing the amount of crosslinker led to an increase in the stretchability of PDMS POFs, in the case of PDMS POFs (15:1) and (20:1).

The tensile modulus also followed a similar trend as the mechanical strength of PDMS POFs, as depicted in Fig. 2b. The PDMS POFs (10:1) had the highest average tensile modulus, whereas PDMS POFs (1:1) and (20:1) exhibited the lowest tensile modulus. The tensile modulus of the PDMS POFs was also influenced by the amount of sol fraction (refer to experimental section for details of the sol fraction calculation) present in PDMS POFs, as displayed in Fig. 2b. The PDMS POFs (10:1) possessed the lowest sol fraction of approximately 4%, whereas PDMS POFs (1:1) possessed the highest sol fraction of approximately 17%.

Fig. 2c represents the relationship between the tensile modulus and the calculated crosslink density (refer to section 2.2, for crosslink density calculations) of the PDMS POFs. The increase in the crosslink density corresponded to the increase in the tensile modulus except for the POF formulation (1:1). This implies that the high amount of crosslinker utilized in the PDMS formulation (1:1) leads to a high amount of sol fraction (i.e., higher percentage of defects in the polymer network) and also a decrease in the crosslink density as compared the PDMS POFs (5:1) and (10:1). The overall mechanical properties of the PDMS POFs extracted from the tensile test and swelling studies are summarized in Table 5.

The mechanical properties such as the elasticity and ultimate tensile strength of a crosslinked polymer system are highly dependent on the polymer network topology and the chemical composi-

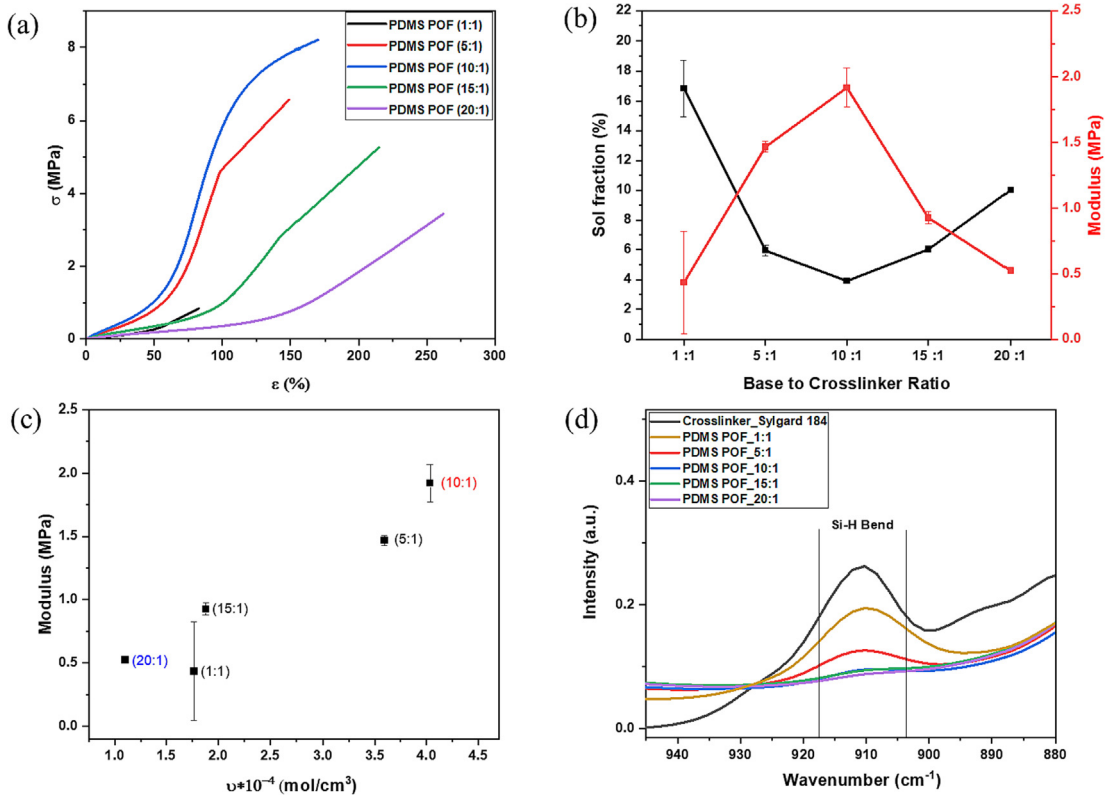

Fig. 2. Effect of base to crosslinker ratio on different properties of soft PDMS POFs. a) Stress–strain behaviour of PDMS POFs cured at 125 °C in a uniaxial tensile test. b) Variation of the tensile modulus and sol fraction with respect to the base to crosslinker ratio (lines in graph are only to guide the eyes). c) Effect of the base to crosslinker ratio on the sol-fraction extracted from the PDMS POFs by the swelling study in toluene. d) Comparison of the ATR-FTIR spectra of the pure crosslinker and crosslinked PDMS POFs.

Table 5
Summary of the mechanical, chemical, and optical properties of PDMS POFs processed at a fixed curing temperature of 125 °C. (*Optical properties of these POFs were not investigated). The superscripts (a–e) identify samples that do not show significant differences for the corresponding property ($p < 0.05$).

POF Formulation Base to Crosslinker Ratio	Tensile modulus (MPa)	Tensile Strength (MPa)	Maximum Elongation (%)	Sol Fraction (%)	Average Crosslink Density $\upsilon * 10^{-4}$ (mol/cm^3)	Light attenuation (dB/cm)
1:1	0.4 ± 0.39^{a}	0.8 ± 0.5^{a}	79 ± 24^{a}	16.82^{a}	1.76	n/a*
5:1	1.5 ± 0.04^{b}	6.6 ± 0.77^{b}	149 ± 25^{b}	5.95^{b}	3.59	0.17 ± 0.002^{ab}
10:1	2.0 ± 0.15^{c}	8.2 ± 0.36^{c}	170 ± 11^{b}	3.90^{c}	3.99	0.14 ± 0.01^{a}
15:1	0.9 ± 0.04^{d}	5.3 ± 0.88^{d}	215 ± 31^{c}	6.03^{b}	1.88	0.18 ± 0.02^{b}
20:1	0.5 ± 0.02	3.4 ± 0.44^{e}	262 ± 19^{d}	9.99^{a}	1.10	n/a*

tion [25]. The ideal polymer network should consist of elastically effective network strands (polymer chains) connected by the junctions (crosslinks). However, the real crosslinked elastomer systems (especially ones prepared from commercially predesigned elastomer kits) always consist of network defects such as dangling chains, loops, sol fraction, unreacted crosslinker, and entanglements along with the elastically effective network [25–29]. The origin of these defects is a function of the stoichiometry of the specific reactive elastomer components, i.e., base, crosslinker, and additives [29]. Despite the long history of research on crosslinked polymer networks, the influence of network defects on the final mechanical properties is still a complex issue that is not clearly understood [30], but we have attempted to provide a hypothesis based on our PDMS POFs.

In this study, commercial PDMS Elastomer Sylgard 184 was utilized for the processing of POFs. Our results show an important relevant aspect of the base to crosslinker ratio, i.e., the stoichiometry of the crosslinkable polymer system. For example, the elastomer system used in this study possesses the highest mechanical properties and crosslink density at a formulation of 10:1. The off-stoichiometry leads to a decrease in the mechanical strength, but on other hand, it leads to an increase in the stretchability for certain formulations too. There is always a compromise between the crosslink density and stretchability of the crosslinkable polymer system [31], as we also found in the case of the crosslinked PDMS based elastomer. This leads to an important conclusion that the same crosslinkable elastomer system, i.e., in this case PDMS, can be tuned to design PDMS POFs with varying stretchability for specific sensing applications, i.e., strain sensing or motion sensing, by simply changing the formulation (stoichiometry).

Based on reported study in literature [32] and our experimental results (Fig. 2), it can be said that the mechanical properties of

crosslinked polysiloxanes are not solely governed by the crosslink density of the system but rather by the combined effect of chemical crosslinks and the amount of defects present in the polymer network.

To further understand the presence of defects such as unreacted crosslinker molecules, ATR-FTIR analysis of PDMS POFs was performed. The peak at 912 cm^{-1} in the ATR-FTIR analysis (Fig. 2d) was utilized as a qualitative indicator to detect the presence of unreacted crosslinker in the PDMS POFs, as it represents the Si-H bending vibrations of the crosslinker molecules [33,34]. PDMS POFs with a formulation of (1:1) and (5:1) possessed the higher amount of unreacted crosslinker (Fig. 2d). This further confirmed the differences in the mechanical strength observed in the PDMS POFs and also highlights the fact that the amount of unreacted crosslinker (i.e., network defect) is another factor that could lead to the degradation of the mechanical properties of PDMS POFs.

The PDMS Sylgard 184 is an example of the hydrosilylation chemistry [35], whose mechanical properties can be significantly influenced by the curing parameters [36] employed during the processing. The effect of the curing temperature and time on the mechanical properties of PDMS POFs was also investigated in this work. For this purpose, the PDMS POFs (10:1) were selected due to their highest mechanical strength. It was observed from uniaxial tensile testing experiments that the tensile strength of PDMS POFs (10:1) increased as the curing temperature increased, as depicted in Fig. S6a. The tensile modulus also increased with increase of curing temperature following similar trend as tensile strength, as described in Fig. S6b. The overall summary of the effect of the curing temperature on the mechanical and optical properties is presented in Table 6.

The increase in the mechanical properties with increasing curing temperature can be attributed to the higher conversion efficiency of the hydrosilylation reaction at higher curing temperatures [37] i.e., the formation of a larger number of covalent crosslinks in the polymer network. The similar behaviour of the mechanical properties with respect to the curing temperature has also been found in other studies [38,39]. Our results highlight the fact that the curing temperature is another valuable parameter to tune the mechanical properties of PDMS POFs. Moreover, low curing temperatures such as 23 °C or room temperature curing could be highly desirable to incorporate temperature sensitive additives or moieties to develop functional soft PDMS POFs for specific sensing applications.

3.3. Optical properties of POFs

Regarding the optical properties of POFs, light attenuation is one of the most important features with regard to the intended applications. The coefficient of light attenuation governs the transmission loss of light within the POF over certain distances. We selected the PDMS POFs (10:1) cured at 125 °C to investigate the effect of wavelength on the optical properties. Fig. 3a shows the digital image of the flexible nature of the PDMS POF transmitting light in a loop configuration around a human finger. The cut-back study data showed, in the case of core only PDMS POFs (10:1), that the light attenuation decreases with the increase in the wavelength of light utilized, as depicted in Fig. 3b. The light attenuation in POFs is highly dependent on the wavelength of the light source used, which is further related to the various intrinsic and extrinsic optical losses.

The intrinsic losses are mainly related to the absorption (via electronic transitions and molecular vibrations) and scattering by the polymer material. The extrinsic losses come from the organic contaminants, dust, and volumetric defects such as pores, bubbles, and surface roughness features due to processing of the POF [40,41]. The absorption losses for the PDMS were dependent on the overtone and combination band molecular vibrations of –CH groups within the range of 600–1600 nm [41]. Moreover, the extrinsic scattering due to the surface roughness of the PDMS waveguide also contributes to the light attenuation [41]. In our case, we found a RMS surface roughness of 28 nm for our PDMS POF (Fig. S4).

Apart from the surface roughness, recently, it has been reported that the surface of the PDMS Sylgard 184 elastomer possesses network mesh structure with a mesh size ranging from 10 to 16 nm [42]. This nanostructure present in the crosslinked PDMS may probably also lead to intrinsic light scattering, i.e., Rayleigh scattering which is inversely proportional to the fourth power of the wavelength. In our study, it was clear that PDMS POFs have higher optical losses at the wavelength of 455 nm and 530 nm. This might be attributed to the combined effect of absorption via the tails of electronic transitions, molecular vibrations of –CH bonds, and Rayleigh scattering, which is lower at the higher wavelengths of 660 and 810 nm compared to 455 and 530 nm.

Moreover, it was also observed that the curing temperature of the PDMS formulation and crosslink density also influence the light attenuation of PDMS POFs, although the effect was smaller than that observed for the mechanical properties (Fig. 3c/Table 6 and Fig. 3d/Table 5, respectively). Only curing at a high temperature (200 °C) led to a significant difference in the light attenuation when compared to the standard formulation (PDMS POF 10:1, 125 °C). The decrease in the crosslink density led to a significant increase in light attenuation in PDMS POFs 15:1 (Fig. 3d), which might be related to the presence of a larger number of polymer network defects such as sol fraction (Table 5) present in this formulation when compared to PDMS POFs (10:1), as explained in the previous section. This study provides evidence that defects in the three-dimensional crosslinked polymer network may also lead to excessive light scattering. In other words, it might be hypothesized that the PDMS polymer network with a high crosslink density transmits light with a lower light attenuation. However, these results provide a promising range of optical properties and specific

Table 6
Summary of the mechanical and optical properties of the PDMS POFs (10:1) with respect to the curing temperature. The samples with same superscripts (a–d) show no significant differences for the corresponding property ($p < 0.05$). The curing parameters (time and temperature) were selected based on the rheology study presented in Fig. S16.

Curing Time	Cure Temperature (°C)	Tensile modulus (MPa)	Tensile Strength (MPa)	Light attenuation (dB/cm)	Elongation ϵ (%)
96 h	23	1.22 ± 0.06^{a}	6.8 ± 0.69^{a}	0.18 ± 0.03^{ab}	206 ± 25^{a}
2.5 h	75	2.06 ± 0.04^{c}	8.1 ± 0.85^{b}	0.15 ± 0.01^{a}	144 ± 27^{b}
37 min	125	1.98 ± 0.15^{b}	8.2 ± 0.36^{b}	0.14 ± 0.01^{a}	170 ± 11^{b}
22 min	200	2.80 ± 0.05^{d}	9.6 ± 0.36^{c}	0.21 ± 0.02^{b}	129 ± 12^{c}

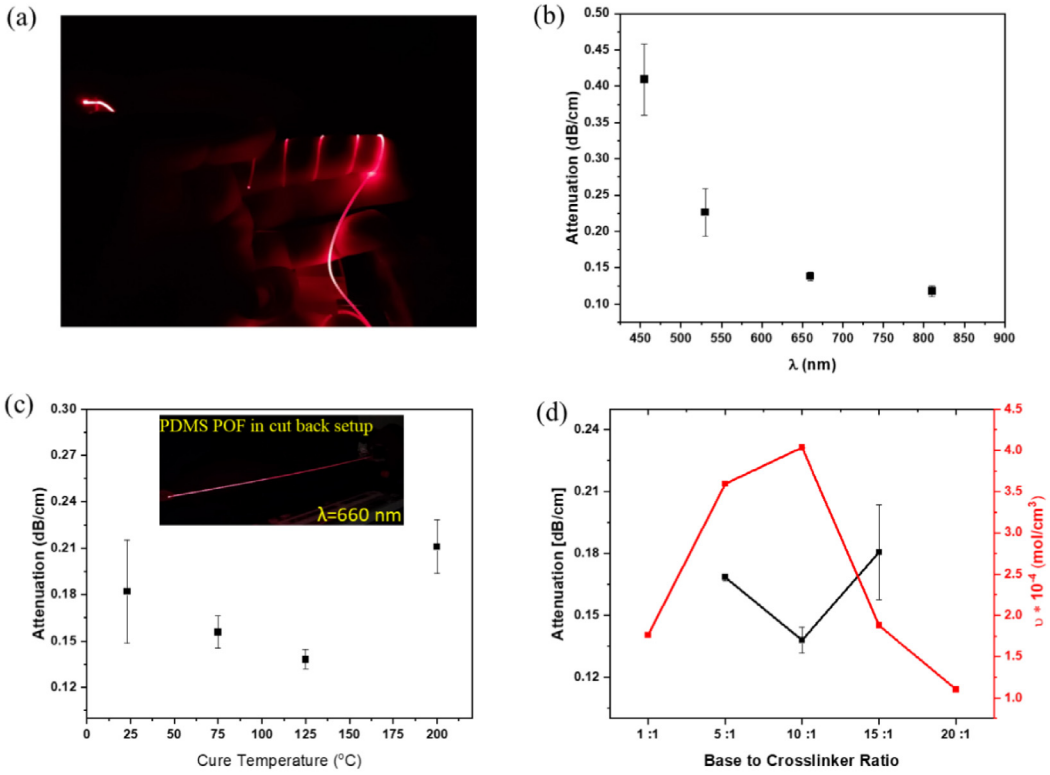

Fig. 3. Optical properties of PDMS POFs. a) Digital image of PDMS POF (10:1) in a bend configuration of loops around the finger, depicting the flexibility and light transmission in real time. b) The variation in the light attenuation of PDMS POFs (10:1) with respect to the wavelength of the light source used. c) The effect of the curing temperature on the light attenuation of PDMS POFs (10:1). d) The variation in the light attenuation and crosslink density of PDMS POFs processed with different base to crosslinker ratios.

wavelength selection (Fig. 3b) for multiple sensing applications especially for biomedical sensing. The high mechanical flexibility and lower light attenuation of our PDMS POFs in the near infrared (NIR) region, i.e., at 810 and 660 nm, combined with near infrared spectroscopy (NIRS) could allow the use of these POFs in the field of oxygenation saturation sensing and neural activity sensing [43,44].

3.4. Core/Clad POFs

Based on the above-mentioned results, we further targeted our study on the development of a robust core/clad system as compared to core only PDMS POFs, which can be employed for sensing applications. The cladding is desirable for the protection of the fiber core from various environmental factors such as humidity, temperature, and dust. The PDMS POF (10:1) cured at 125 °C was selected as the core material due to the good combination of mechanical strength and low light light attenuation, whereas the fluoropolymer THV was selected as the cladding material due to its low refractive index. The dip coating of the PDMS POF in the THV polymer solution led to the formation of a thin THV cladding (~10 μm), as shown in Fig. 1b. For the visual confirmation of the formation of a uniform THV cladding, PDMS POFs were dip coated in the THV polymer solution dispersed with Lumogen Red dye. THV formed a uniform coating as the cladding on the surface of the PDMS core (Fig. 4a). As a comparison, the PDMS POF dip coated in only Lumogen Red dye solution formed non-uniform aggregates of dye partially over its surface (Fig. 4a).

Furthermore, the presence of the THV cladding (without dye) was also detected with the ATR-FTIR technique. Fig. 4b shows the comparative analysis of the FTIR spectra of the core only and core/clad based POFs. The emergence of new peaks at 1398 cm^{-1} and in between 1130 and 1200 cm^{-1} were associated to the polymer THV. The peaks between 1130 and 1200 cm^{-1} were attributed to the stretching vibrations of the C-F bond [45,46], whereas the peak at 1398 cm^{-1} was linked to the CH_2 bending vibrations in THV [46]. These results further confirmed the presence of the THV cladding in core/clad PDMS POFs.

The uniaxial tensile testing results revealed the higher tensile strength in PDMS/THV POFs (9.6 ± 0.28 MPa, $p < 0.05$) in comparison to core only PDMS POFs (8.2 ± 0.36 MPa, $p < 0.05$), as represented in Fig. 4c. The understanding of this behavior came from the heat treatment (HT) of the PDMS/THV POFs. The dip coated PDMS/THV POFs were subjected to HT at 110 °C for 20 min to ensure the solvent removal from the THV cladding and uniform THV coating formation. To understand if the enhancement of the mechanical strength was either due to the thin THV cladding or due to the HT of the PDMS core, we performed the HT of the core only PDMS POFs at the same conditions as the PDMS/THV (core/clad) POFs. The tensile testing data shown in Fig. 4c showed an interesting result, which confirmed that the enhancement of the tensile modulus and ultimate tensile strength can be attributed to the HT of the PDMS core. The HT of the PDMS core might lead to further crosslinking inside the POF, which may be related to the enhanced mechanical strength. Our HT experiments provides evidence that despite crosslinking the PDMS at optimum curing conditions, some unreacted crosslinker molecules remain in the cured samples, which further leads to post crosslinking of PDMS during the heat treatment process, resulting in the enhanced strength of the crosslinked polymer. Our results can be supported by other studies, which found similar results on the post HT of PDMS elastomers [47,48]. The optical characterization of PDMS/THV (core/clad) POFs showed no significant difference in the average light attenuation compared to core only PDMS POFs (Fig. S7),

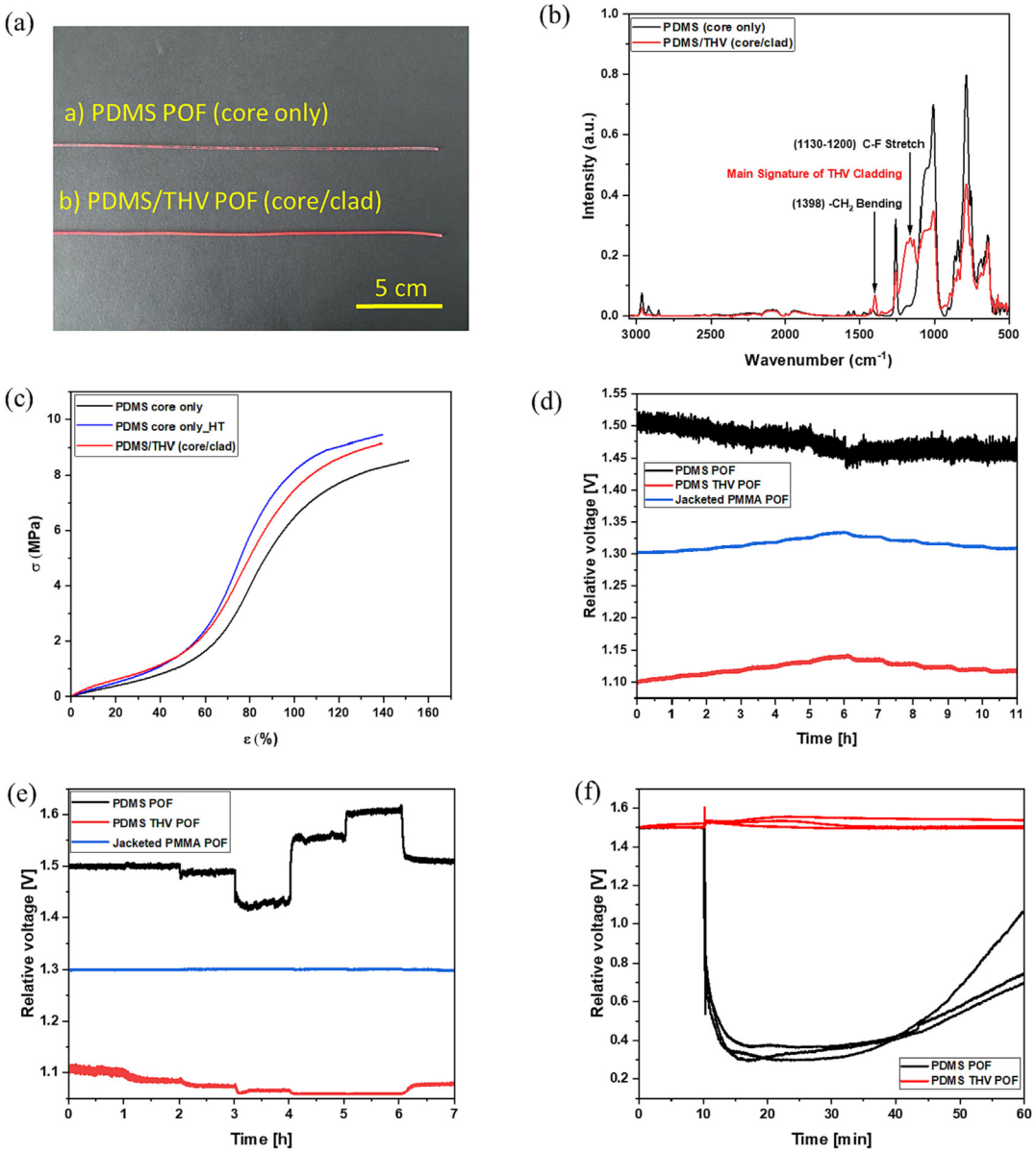

Fig. 4. Properties of PDMS/THV (core/clad) POFs. a) Digital image of the PDMS core only and PDMS/THV (core/clad) coated with Lumogen Red Dye. b) ATR FTIR spectra of PDMS POF and PDMS/THV POFs. c) Stress–strain response of PDMS/THV POFs compared to as processed and heat treated core only PDMS POFs. d) Fiber response to changing climatic conditions; results of the temperature sensitivity of POFs. e) Results of the humidity sensitivity of POFs. f) Results of the water droplet tests. Water was sprayed on the POFs after 10 min of measurement. (For interpretation of the references to colour in this figure legend, the reader is referred to the web version of this article.)

i.e., PDMS core only and PDMS/THV POFs have similar optical performance. The increased variability in attenuation of PDMS/THV POFs is due to the dip coating process leading to some irregularities in the thickness of the cladding. However, as it will be shown later, this does not affect the performance of core/clad fibers.

3.5. Sensing application of PDMS POFs

After the characterization of PDMS and PDMS/THV based POFs, we selected core only PDMS (10:1) POFs cured at 125 °C and PDMS/THV (core/clad) POFs for the sensing application due to their better mechanical strength and lower light light attenuation as comparison to the other soft POFs developed in this work. The goal of our study was to demonstrate the development of a soft POF based pressure sensor targeted for continuous, real time monitoring of pressure subjected to skin tissue in certain human body postures, for example, pressure on skin tissue while a person is sitting on a chair for long time or the pressure on skin tissue while a person is laying on a bed mattress for a long time, i.e., patients in hospitals. In the above mentioned application scenarios where PDMS POFs need to be placed next to human skin tissue, changes in various environmental factors such as temperature (T), relative humidity (RH), or body fluids such as body sweat could influence the optical performance of PDMS POFs. This makes it very important to understand the influence of environmental factors on soft PDMS POFs before the textile integration process. We conducted an analysis of the PDMS POF response against changing climatic conditions (temperature and relative humidity) as well as when in contact with liquid water.

To assess the effect of RH and T, a jacketed commercial POF was also used as a reference to minimize the effect of the electronic signals. We observed a stable signal for the three POFs during the variation of the temperature from 30 to 45 °C (Fig. 4d). Statistical analysis (Table S1) indicated no significant effect of either the tem-

perature or the fiber type on the signal. A different behaviour was found for the RH tests (Fig. 4e). Here, core only PDMS POFs were significantly affected by the RH. In comparison, the PDMS/THV POFs have a relatively constant signal and a performance similar to jacketed PMMA. Our study revealed a significant effect of the fiber type, with PDMS core only POF performing inferior to the other two POFs especially after 4 h of RH testing (Table S2).

The protective role of the THV cladding was further confirmed by the spray test, in which water droplets were sprayed on the surface of POFs to monitor the real time change in the light intensity of POFs. Once sprayed with water droplets, PDMS core only and PDMS/THV POFs displayed a big difference in the behavior, confirming the results of the environmental factors mentioned above. PDMS core only POFs were highly sensitive to the presence of water droplets on their surface, showing a sudden decrease in the light intensity initially (Fig. 4f) and then a slow return to the original value after approximately 25 min. This effect can be clearly attributed to the scattering of light by water droplets on the POF

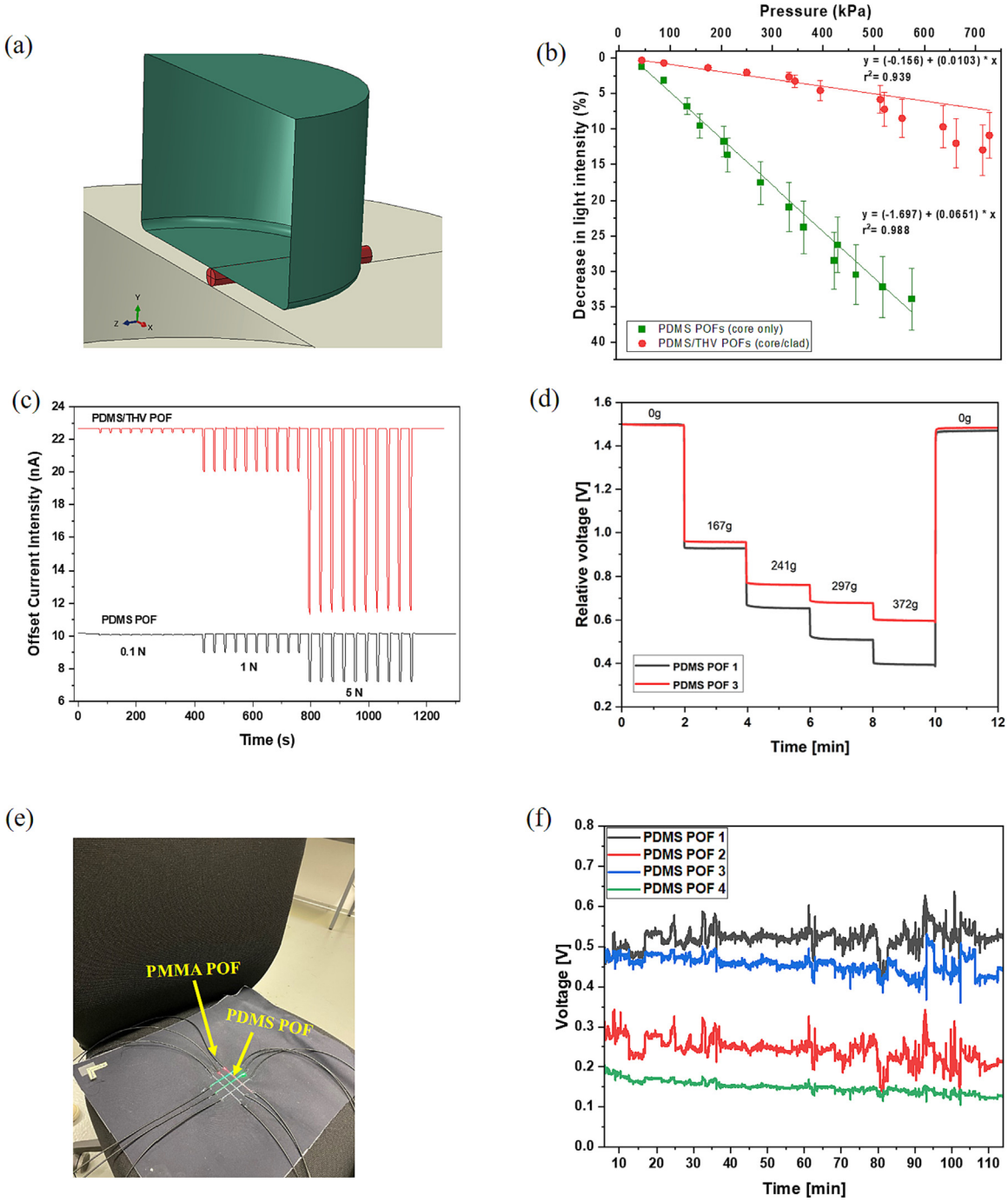

Fig. 5. Soft POFs response to load. a) Three dimensional model of the plunger and soft POF simulating the experimental set up used for the compression test. b) Pressure sensing response of PDMS and PDMS/THV POFs. Data is expressed as mean ± s.d, n = 3. The linear fitting curves were obtained via weighted linear fit in the software Origin 2022. c) Cyclic response of PDMS and PDMS/THV POFs. See Figures S10 and S11 for raw signal data d) Response of PDMS POFs to load sensitivity. The loads were applied on the fiber crossing integrated into a patch of 3 × 3 fibers. See Figures S13 and S14 for other examples of crossover points using both PDMS POFs and PDMS/THV POFs. e) Photo of the PDMS patch placed on a chair for real time sensing application. f) Real time raw data of the subject sitting on the PDMS patch (The PDMS patch of 3 × 3 fibers was placed on a chair).

surface, which disappeared after some time due to the evaporation of water droplets (Fig. 4f). On the other hand, the detected light intensity in PDMS/THV POFs was unaffected (Fig. 4f) by the presence of water droplets. The THV cladding prevented the direct contact of water droplets with the PDMS core, inhibiting the light scattering loss effect by water droplets. The effect was not due to a higher hydrophobicity, as both POFs show a strong hydrophobic behavior, as visualized in Fig. S8. It can be concluded that the cladding plays an important role in the detection of the stable light intensity signals in POFs.

Our results demonstrate that the thin THV cladding is an effective option that could be easily applied for the protection of the PDMS POFs against environmental factors. The THV cladding system is not only limited to PDMS but could also be optimized and extended for other POF materials depending on the required application.

The force and pressure sensing performance of the PDMS and PDMS/THV POFs was determined via cyclic compression testing (details of method and set up in section 2.3.4 and Fig. S17). Fig. S22 represents the force versus light intensity relationship of PDMS and PDMS/THV POFs i.e. force sensing response. Both POFs were successfully able to sense all the forces within the range of 0.1 to 5 N. However, PDMS core only POFS are more sensitive to all loads within this range as compared to PDMS/THV POFs. Fig. 5a shows three dimensional model of the fiber and plunger system utilized for FEM simulation of the compression test and Fig. S21 shows the snapshot of the FEM simulation describing the change in effective contact area between plunger and soft PDMS POF during compression test (more information in Table S5 and Video S1). The FEM data was utilized to calculate the pressure on PDMS POFs. Fig. 5b describes the relationship between pressure versus light intensity signal of PDMS and PDMS/THV POFs. Both POFs exhibited linear response between pressure and the decrease of light intensity signal (Fig. 5b). However, pressure sensing behaviour of PDMS/THV POFs (Fig. 5b) clearly describes the advantage of THV cladding, which provides higher accuracy acts as direct contact to the measured stimulus i.e. pressure, providing lower light losses as compared to PDMS core-only POFs. Indeed, the apparent higher pressure sensitivity of PDMS POFs is in fact due to an increased light out-coupling to the environment, as the plunger and bottom plate works as cladding for these POFs. Another advantage refers to the range of pressures that can be detected accurately, that is, with low signal variability. This range extends to 300 kPa for PDMS/THV POFs as compared to only 100 kPa in case of PDMS POFs. The cyclic performance of the PDMS and PDMS/THV POFs was also tested at 3 different loads of 0.1 N, 1 N and 5 N. Fig. 5c describes the cyclic response of the PDMS POFs in comparison to PDMS/THV POFs (raw signal data in Fig. S10 and Fig. S11). Both PDMS POF as well as PDMS/THV POF provided similar signal response during each successive cycle at all 3 loadings (Fig. 5c), which reveals the reproducible optical signal response of these soft POFs.

However, the decay of the light intensity in the case of PDMS/THV POFs was always smaller compared to PDMS core only POFs, which can be attributed to the reduction in the light out-coupling due to the presence of the THV cladding.

To demonstrate the versatility of PDMS POFs and PDMS/THV POFs, we developed demonstrator patches via textile integration. A 3 × 3 matrix configuration of POFs with 9 fiber crossover points was fabricated via stitching (Fig. S1) of POFs into a textile patch. The evaluation of the sensitivity of this demonstrator was analysed by application of different loads on crossover points of PDMS POFs. Fig. 5d displays the change in the detected relative voltage signal on the application of load at the single fiber crossing point, i.e., the crossing of PDMS POF 1 and PDMS POF 3. It was found again that the detected signal of the PDMS POFs decreases as the applied load increases. The similar kind of optical loss mechanism at the POF crossing point has been found in another study [49]. Similar results were obtained for other crossing points, for both types of POFs (Figs. S13 and S14).

The demonstrator patch made of 3 × 3 PDMS POF matrix was further tested to check its wearable health monitoring potential in real time. We tested the pressure variations on skin tissue, i.e., on the buttocks of the subject sitting on a chair. The patch was placed on a chair, as shown in Fig. 5e. Then, the subject sat on the patch during the measurement and performed computer activities. This implies that during the measurement, the subject stayed seated on the patch with natural body movements.

Fig. 5f represents the real time raw data recorded due to the body movements and load applied by the subject on the demonstrator patch. Interestingly, it was found that all the PDMS POFs in the patch detect the same human movements, i.e., pressure variations with different intensities. As a comparison, Fig. S9 shows patches with both types of PDMS POFs under long-term and static loading conditions. The signal was constant for 15 h and then returned to the original value upon removal of the load (Fig. S9). The lack of reconvergence of the light signal for the PDMS/THV fibers (Fig. S9) could be due to different effects. First, due to the movement and misalignment of the connection between PDMS/THV POF and commercial PMMA POF (see Fig. 5e) during the removal of the load, which lead to a residual light loss. Second, the long term loading might have led to local debonding of the THV cladding (Fig. S23), which could contribute to additional light losses and consequent lack of reconvergence of the light signal in PDMS/THV POFs as well as to instability in the cycling testing for large loads (5 N, Fig. S11) or decreased longevity of these POFs. The connection of the soft and anti-adherent PDMS POFs to both commercial PMMA POFs and to cladding materials is a challenging point in our sensor design that is still under improvement.

The differences in the signal intensities with different PDMS POFs in the textile patch (Fig. 5f) can be explained by the fact that POFs were compressed differently depending on their location at the crossing points in the patch and as well as on the point of application of the load, implying non uniform deformation of different PDMS POFs (Fig. 5f). This test was, therefore, a proof of concept of this wearable health monitoring patch because PDMS POFs were successfully able to detect human movements, which indirectly could be further translated to pressure variations.

4. Conclusion

This study has demonstrated the processing-structure relationship of core only soft PDMS POFs and core/clad (PDMS/THV) POFs. The combination of moulding in tube strategy and dip coating provides a fast and facile approach to the processing of core only or core/clad POFs with mechanical and optical properties on par with state of the art. The mechanical and optical properties of these elastic core only PDMS POFs can be tuned by the proper selection of the right chemical formulation of PDMS (i.e., base to crosslinker ratio) and processing parameters such as curing temperature and curing time. The combination of low optical light attenuation and tunable elastomeric-like mechanical properties makes this platform particularly relevant for biomedical applications. Furthermore, PDMS/THV POFs (core/clad) have been developed by the dip coating process and heat treatment (HT) of the THV cladding. The dip coating process provided a thin, protective THV cladding, and HT led to the enhancement of the mechanical strength of core/clad POFs. The developed soft POFs in this work demonstrated the load and pressure sensing capability with sensitivity to loads as low as 0.1 N and highly accurate pressure sensing up to 300 kPa respectively. Moreover, the PDMS POFs were successfully inter-

gated into the textile patch, which was used to successfully demonstrate the continuous measurements of human body movements in real time. Our study revealed the full property space of PDMS based POFs and will allow researchers to tailor the mechanical and optical properties of these POFs on demand, as required in sensing applications. Moreover, the processing parameters of this work are not only limited to POFs but could also be harnessed to process and design various kinds of optical sensors from biomedical to soft robotics based applications in the form of PDMS films or other design configurations.

Data availability

Data will be made available on request.

Declaration of Competing Interest

The authors declare that they have no known competing financial interests or personal relationships that could have appeared to influence the work reported in this paper.

Acknowledgments

The work was supported by the Swiss National Science Foundation (SNSF) and Innosuisse BRIDGE Discovery funding opportunity (project number 40B2-0_180983). We would also like to thank Abdul-Rahman Asaad and Corinne Jung from Laboratoire de Physique et Mécanique Textiles (LPMT), Université de Haute-Alsace (UHA) for textile integration of PDMS POFs via embroidery.

Appendix A. Supplementary data

Supplementary data to this article can be found online at https://doi.org/10.1016/j.matdes.2023.112115.

References

[1] A.G. Leal-Junior, C.A.R. Diaz, L.M. Avellar, M.J. Pontes, C. Marques, A. Frizera, Polymer optical fiber sensors in healthcare applications: a comprehensive review, Sensors 19 (14) (2019) 3156.
[2] Y. Yamada, Textile-integrated polymer optical fibers for healthcare and medical applications, Biomed. Phys. Eng. Express 6 (6) (2020) 062001.
[3] K.-P. Lee, J. Yip, K.-L. Yick, C. Lu, C.K. Lo, Textile-based fiber optic sensors for health monitoring: a systematic and citation network analysis review, Textile Res. J., 00405175211036206.
[4] Z.S. Ballard, A. Ozcan, Wearable optical sensors, in: J.M. Rehg, S.A. Murphy, S. Kumar (Eds.), Mobile Health, Springer International Publishing, Cham, 2017, pp. 313–342.
[5] S. Mirjalali, S. Peng, Z. Fang, C.H. Wang, S. Wu, Wearable sensors for remote health monitoring: potential applications for early diagnosis of Covid-19, Adv. Mater. Technol. 7 (1) (2022) 2100545.
[6] K. Meng, X. Xiao, W. Wei, G. Chen, A. Nashalian, S. Shen, X. Xiao, J. Chen, Wearable pressure sensors for pulse wave monitoring, Adv. Mater. 34 (21) (2022) 2109357.
[7] B.M. Quandt, L.F. Boesel, R.M. Rossi, Polymer optical fibers in healthcare: solutions, applications and implications. A perspective, Polym. Int. 67 (9) (2018) 1150–1154.
[8] B.M. Quandt, L.J. Scherer, L.F. Boesel, M. Wolf, G.-L. Bona, R.M. Rossi, Body-monitoring and health supervision by means of optical fiber-based sensing systems in medical textiles, Adv. Healthc. Mater. 4 (3) (2015) 330–355.
[9] M. Krehel, M. Wolf, L.F. Boesel, R.M. Rossi, G.-L. Bona, L.J. Scherer, Development of a luminous textile for reflective pulse oximetry measurements, Biomed. Opt. Express 5 (8) (2014) 2537–2547.
[10] B.M. Quandt, F. Braun, D. Ferrario, R.M. Rossi, A. Scheel-Sailer, M. Wolf, G.-L. Bona, R. Hufenus, L.J. Scherer, L.F. Boesel, Body-monitoring with photonic textiles: a reflective heartbeat sensor based on polymer optical fibers, J. R. Soc. Interface 14 (128) (2017) 20170060.
[11] B.M. Quandt, M.S. Pfister, J.F. Lübben, F. Spano, R.M. Rossi, G.-L. Bona, L.F. Boesel, POF-yarn weaves: controlling the light out-coupling of wearable phototherapy devices, Biomed. Opt. Express 8 (10) (2017) 4316–4330.
[12] B.M. Quandt, R. Hufenus, B. Weisse, F. Braun, M. Wolf, A. Scheel-Sailer, G.-L. Bona, R.M. Rossi, L.F. Boesel, Optimization of novel melt-extruded polymer optical fibers designed for pressure sensor applications, Eur. Polym. J. 88 (2017) 44–55.
[13] L. Meng, A.P.F. Turner, W.C. Mak, Soft and flexible material-based affinity sensors, Biotechnol. Adv. 39 (2020). 107398.
[14] J. Guo, C. Yang, Q. Dai, L. Kong, Soft and stretchable polymeric optical waveguide-based sensors for wearable and biomedical applications, Sensors 19 (17) (2019) 3771.
[15] J. Guo, M. Niu, C. Yang, Highly flexible and stretchable optical strain sensing for human motion detection, Optica 4 (10) (2017) 1285–1288.
[16] F.A. Reifler, R. Hufenus, M. Krehel, E. Zgraggen, R.M. Rossi, L.J. Scherer, Polymer optical fibers for textile applications – bicomponent melt spinning from cyclic olefin polymer and structural characteristics revealed by wide angle X-ray diffraction, Polymer 55 (22) (2014) 5695–5707.
[17] K. Jakubowski, R. Hufenus, J. Smajic, M. Heuberger, Bicomponent melt-spinning of polymer optical fibers, Advanced Photonics 2018 (BGPP, IPR, NP, NOMA, Sensors, Networks, SPPCom, SOF), Optica Publishing Group, Zurich, 2018, p. JTu5A.78.
[18] A. Leber, B. Cholst, J. Sandt, N. Vogel, M. Kolle, Stretchable thermoplastic elastomer optical fibers for sensing of extreme deformations, Adv. Funct. Mater. 29 (5) (2019) 1802629.
[19] Y. Qu, T. Nguyen-Dang, A.G. Page, W. Yan, T. Das Gupta, G.M. Rotaru, R.M. Rossi, V.D. Favrod, N. Bartolomei, F. Sorin, Superelastic Multimaterial Electronic and Photonic Fibers and Devices via Thermal Drawing, Adv. Mater. 30(27) (2018) 1707251.
[20] M. Hohberg, D. Siebler, P. Rohwetter, Production process and characterization of sensitized all elastomeric POF, POF 2015–24th International conference on plastic optical fibers (Proceedings), Nuremberg, Germany, 2015, pp. 91–94.
[21] T. Flipsen, A. Pennings, G. Hadziioannou, Polymer optical fiber with high thermal stability and low optical losses based on novel densely crosslinked polycarbosiloxanes, J. Appl. Polym. Sci. 67 (13) (1998) 2223–2230.
[22] J. Guo, B. Zhou, C. Yang, Q. Dai, L. Kong, Stretchable and Temperature-Sensitive Polymer Optical Fibers for Wearable Health Monitoring, Adv. Funct. Mater. 29 (33) (2019) 1902898.
[23] M. Chen, Z. Wang, K. Li, X. Wang, L. Wei, Elastic and stretchable functional fibers: A review of materials, fabrication methods, and applications, Adv. Fiber Mater. 3 (1) (2021) 1–13.
[24] W. Chassé, M. Lang, J.-U. Sommer, K. Saalwächter, Cross-link density estimation of PDMS networks with precise consideration of networks defects, Macromolecules 45 (2) (2012) 899–912.
[25] Y. Gu, J. Zhao, J.A. Johnson, A (macro) molecular-level understanding of polymer network topology, Trends Chem. 1 (3) (2019) 318–334.
[26] M. Zhong, R. Wang, K. Kawamoto, B.D. Olsen, J.A. Johnson, Quantifying the impact of molecular defects on polymer network elasticity, Science 353 (6305) (2016) 1264–1268.
[27] K. Urayama, Network topology–mechanical properties relationships of model elastomers, Polym. J. 40 (8) (2008) 669–678.
[28] K. Urayama, T. Kawamura, S. Kohjiya, Structure–mechanical property correlations of model siloxane elastomers with controlled network topology, Polymer 50 (2) (2009) 347–356.
[29] P. Mazurek, S. Vudayagiri, A.L. Skov, How to tailor flexible silicone elastomers with mechanical integrity: a tutorial review, Chem. Soc. Rev. 48 (6) (2019) 1448–1464.
[30] T. Fujiyabu, N. Sakumichi, T. Katashima, C. Liu, K. Mayumi, U.-I. Chung, T. Sakai, Tri-branched gels: Rubbery materials with the lowest branching factor approach the ideal elastic limit, Sci. Adv. 8 (14) (2022) eabk0010.
[31] Y. Takeoka, S. Liu, F. Asai, Improvement of mechanical properties of elastic materials by chemical methods, Sci. Technol. Adv. Mater. 21 (1) (2020) 817–832.
[32] J.D. Glover, C.E. McLaughlin, M.K. McFarland, J.T. Pham, Extracting uncrosslinked material from low tensile modulus sylgard 184 and the effect on mechanical properties, J. Polym. Sci. 58 (2) (2020) 343–351.
[33] A. Zhang, L. Cheng, S. Hong, C. Yang, Y. Lin, Preparation of anti-fouling silicone elastomers by covalent immobilization of carboxybetaine, RSC Adv. 5 (107) (2015) 88456–88463.
[34] J. González-Rivera, R. Iglio, G. Barillaro, C. Duce, M.R. Tinè, Structural and thermoanalytical characterization of 3D porous PDMS foam materials: the effect of impurities derived from a sugar templating process, Polymers 10 (6) (2018) 616.
[35] D. Troegel, J. Stohrer, Recent advances and actual challenges in late transition metal catalyzed hydrosilylation of olefins from an industrial point of view, Coord. Chem. Rev. 255 (13) (2011) 1440–1459.
[36] I.-K. Hong, S. Lee, Cure kinetics and modeling the reaction of silicone rubber, J. Ind. Eng. Chem. 19 (1) (2013) 42–47.
[37] T. Bardelli, C. Marano, F. Briatico Vangosa, Polydimethylsiloxane crosslinking kinetics: a systematic study on Sylgard184 comparing rheological and thermal approaches, J. Appl. Polym. Sci. 138 (39) (2021) 51013.
[38] J. Vaicekauskaite, P. Mazurek, S. Vudayagiri, A. Ladegaard Skov, Silicone elastomer map: design the ideal elastomer, SPIE2019.
[39] I.D. Johnston, D.K. McCluskey, C.K.L. Tan, M.C. Tracey, Mechanical characterization of bulk Sylgard 184 for microfluidics and microengineering, J. Micromech. Microeng. 24 (3) (2014) 035017.
[40] Y. Koike, Fundamentals of plastic optical fibers, John Wiley & Sons, 2015.
[41] D. Cai, H.M. Heise, Spectroscopic aspects of polydimethylsiloxane (PDMS) used for optical waveguides, Molecular Spectroscopy—Experiment and Theory, Springer, 2019, pp. 401–425.
[42] V. Drebezghova, H. Gojzewski, A. Allal, M.A. Hempenius, C. Nardin, G.J. Vancso, Network mesh nanostructures in cross-linked poly(dimethylsiloxane) visualized by AFM, Macromol. Chem. Phys. 221 (17) (2020) 2000170.

[43] A. Sakudo, Near-infrared spectroscopy for medical applications: current status and future perspectives, Clin. Chim. Acta 455 (2016) 181–188.
[44] R. Nazempour, B. Zhang, Z. Ye, L. Yin, X. Lv, X. Sheng, Emerging applications of optical fiber-based devices for brain research, Adv. Fiber Mater. 4 (1) (2022) 24–42.
[45] C. Slim, E. Ratajovà, S. Griveau, F. Kanoufi, D. Ferraro, C. Perréard, F. d'Orlyé, A. Varenne, F. Bedioui, Two-step local functionalization of fluoropolymer Dyneon THV microfluidic materials by scanning electrochemical microscopy combined to click reaction, Electrochem. Commun. 60 (2015) 5–8.
[46] Y. Zhang, B. Yang, K. Li, D. Hou, C. Zhao, J. Wang, Electrospun porous poly (tetrafluoroethylene-co-hexafluoropropylene-co-vinylidene fluoride) membranes for membrane distillation, RSC Adv. 7 (89) (2017) 56183–56193.
[47] R. Seghir, S. Arscott, Extended PDMS stiffness range for flexible systems, Sens. Actuators, A 230 (2015) 33–39.
[48] Z. Brounstein, J. Zhao, D. Geller, N. Gupta, A. Labouriau, Long-term thermal aging of modified Sylgard 184 formulations, Polymers 13 (18) (2021) 3125.
[49] C.-A. Bunge, J.P. Kallweit, M. Al Houri, B. Mohr, A. Bērziòš, C. Grauberger, P. Adi, T. Gries, Textile multitouch force-sensor array based on circular and non-circular polymer optical fibers, IEEE Sens. J. 20 (14) (2020) 7548–7555.